**Atmospheric
Measurement
Techniques**

Comparison of methods for the determination of NO-O$_3$-NO$_2$ fluxes and chemical interactions over a bare soil

P. Stella[1,*], B. Loubet[1], P. Laville[1], E. Lamaud[2], M. Cazaunau[3], S. Laufs[4], F. Bernard[3], B. Grosselin[3], N. Mascher[1], R. Kurtenbach[4], A. Mellouki[3], J. Kleffmann[4], and P. Cellier[1]

[1]National Institute for Agronomic Research (INRA), UMR EGC, Thiverval-Grignon, France
[2]National Institute for Agronomic Research (INRA), UR EPHYSE, Villenave d'Ornon, France
[3]Institut de Combustion, Aérothermique, Réactivité et Environnement, ICARE-CNRS, Orléans, France
[4]Physikalische Chemie, FB C, Bergische Universität Wuppertal, Wuppertal, Germany
[*]now at: Max Planck Institute for Chemistry, Biogeochemistry Department, P.O. Box 3060, 55020 Mainz, Germany

Correspondence to: P. Stella (patrick.stella@mpic.de)

Abstract. Tropospheric ozone (O$_3$) is a known greenhouse gas responsible for impacts on human and animal health and ecosystem functioning. In addition, O$_3$ plays an important role in tropospheric chemistry, together with nitrogen oxides. The determination of surface-atmosphere exchange fluxes of these trace gases is a prerequisite to establish their atmospheric budget and evaluate their impact onto the biosphere. In this study, O$_3$, nitric oxide (NO) and nitrogen dioxide (NO$_2$) fluxes were measured using the aerodynamic gradient method over a bare soil in an agricultural field. Ozone and NO fluxes were also measured using eddy-covariance and automatic chambers, respectively. The aerodynamic gradient measurement system, composed of fast response sensors, was capable to measure significant differences in NO and O$_3$ mixing ratios between heights. However, due to local advection, NO$_2$ mixing ratios were highly non-stationary and NO$_2$ fluxes were, therefore, not significantly different from zero. The chemical reactions between O$_3$, NO and NO$_2$ led to little ozone flux divergence between the surface and the measurement height (less than 1 % of the flux on average), whereas the NO flux divergence was about 10 % on average. The use of fast response sensors allowed reducing the flux uncertainty. The aerodynamic gradient and the eddy-covariance methods gave comparable O$_3$ fluxes. The chamber NO fluxes were down to 70 % lower than the aerodynamic gradient fluxes, probably because of either the spatial heterogeneity of the soil NO emissions or the perturbation due to the chamber itself.

1 Introduction

Tropospheric ozone (O$_3$) is a common greenhouse gas responsible for a non-negligible part of the radiative forcing (IPCC, 2007). In addition, O$_3$ is a major pollutant having impacts on human (and animal) health and ecosystem functioning (PORG, 1997; Paoletti, 2005; Paoletti and Grulke, 2005; Ainswoth, 2008; Wittig et al., 2009). Since the 1950s, background O$_3$ mixing ratios have doubled and the annual average O$_3$ mixing ratio ranges from 20 to 45 ppb, depending on the geographical location (Vingarzan, 2004). The current global scale pollution models predict an increase in O$_3$ mixing ratios by a factor of 2–4 in the coming century (Vingarzan, 2004). Based on recent ecosystem modelling studies, which include O$_3$ impacts on plants, it is thought that this increase in O$_3$ would lead to a decrease in CO$_2$ absorption by terrestrial ecosystems, which would provide a positive feedback in the atmospheric greenhouse gas budget (Felzer et al., 2007; Sitch et al., 2007).

Nitrogen oxides (NO$_x$ = NO + NO$_2$) are well known for their major role in tropospheric chemistry, in particular for their contribution to the photochemical formation of O$_3$ (Fowler et al., 1998, 1999) and, thus, their indirect contribution to global warming. Nitrogen oxides are released into the atmosphere from a variety of sources; the major being fossil fuel combustion and biomass burning. However, soil microbial emissions are also of high interest, especially as they are diffusive sources which, therefore, affect the atmospheric chemistry over large areas (Delmas et al., 1997). Global NO$_x$ emissions have increased from 12 Tg$_{N-NO_x}$ yr^{-1}

during the pre-industrial area to 40–50 Tg$_{\text{N-NO}_x}$ yr^{-1} actually (Denman et al., 2007). Soil nitric oxide (NO) emissions from agricultural soils are estimated to represent 40 % of the total soil NO emission (Yienger and Levy, 1995; Aneja and Robarge, 1996). Soil nitric oxide emissions occur mainly through the nitrification and denitrification processes and depend on several factors, such as the amount of nitrogen, the soil temperature and the soil moisture (Laville et al., 2009).

The extent to which terrestrial ecosystems intervene in the atmospheric budget of O$_3$ and NO$_x$ is of high interest. Several studies have been performed to understand and evaluate the capacity of ecosystems to represent sources or sinks for O$_3$ (Lamaud et al., 2002, 2009; Zhang et al., 2002, 2006; Altimir et al., 2004, 2006; Gerosa et al., 2004; Rummel et al., 2007; Coyle et al., 2009) and NO$_x$ (Butterbach-Bahl et al., 2002; Rummel et al., 2002; Fang and Mu, 2007; Li and Wang, 2007; Sanchez-Martin et al., 2008; Laville et al., 2009, 2011).

Several methods are known to measure trace gas fluxes between the atmosphere and the biosphere. Among the numerous techniques used, it is possible to distinguish between the direct micrometeorological methods (such as the eddy-covariance (EC) and the disjunct eddy-covariance), the indirect micrometeorological methods (such as the aerodynamic gradient method (AGM), the profile methods and the relaxed eddy-accumulation) (Foken, 2008), and the chamber methods (Meixner et al., 1997; Denmead, 2008). The micrometeorological methods allow measurements at the landscape scale (from a few hectares to several square kilometres), whereas chambers represent the smallest scale (around 1 m^2). The eddy-covariance method has been extensively used for studying carbon dioxide and water vapour exchanges in a network of flux measurement sites such as CarboEuroFlux, (Aubinet et al., 2000), AmeriFlux (Running et al., 1999), Fluxnet (Baldocchi et al., 2001), CarboEurope-IP (Dolman et al., 2006) and NitroEurope-IP (Skiba et al., 2009) and became the reference method for flux measurements. Nevertheless, for trace gases for which there is a lack of fast response sensors, such as NH$_3$, the use of aerodynamic gradient method is still a reference method (e.g., Milford et al., 2009). Moreover, estimating the fluxes of chemically reactive species, especially O$_3$, NO and NO$_2$, requires measuring both the mixing ratios and the fluxes at several heights to estimate the flux divergence due to chemical reactions (Kramm et al., 1991, 1995; Duyzer et al., 1995). Although the EC method could be applied to measure simultaneously the flux at several heights, it is costly, since it requires several fast analysers. Thus, the AGM represents the simplest and cheapest alternative. Nevertheless, there are only few studies reporting comparisons of measurement methods, especially for O$_3$ and NO$_x$, and some of them report contradictory results. As an example, Muller et al. (2009) found a large overestimation in O$_3$ deposition with the AGM when compared to the EC method, whereas Keronen et al. (2003) reported similar O$_3$ fluxes with these two methods. In addition, the few published compari-

son studies (Droppo, 1985; Mikkelsen et al., 2000; Keronen et al., 2003; Muller et al., 2009) did not correct the fluxes for chemical reactions before comparing the different methods.

This study reports measurements of NO-O$_3$-NO$_2$ fluxes over an agricultural field after wheat harvest, tillage and slurry incorporation. The aim of this study was to measure NO-O$_3$-NO$_2$ fluxes by the AGM with a profile system, composed only of fast response sensors. A strong emphasis was given to the quality and uncertainty estimation of the fluxes, as well as on the impact of chemistry between NO$_x$ and O$_3$ on the flux divergences. The results of the AGM are compared with O$_3$ fluxes measured by eddy-covariance and with NO fluxes measured using automatic chambers.

2   Materials and methods

2.1   Site description and meteorological measurements

The experimental site is an agricultural field located at Grignon (48°51′ N, 1°58′ E), 40 km west of Paris. The size of the field is 19 ha with a winter wheat-maize-winter barley-mustard rotation. The soil is a silt loam (31 % clay, 62.5 % silt and 6.5 % sand). The site is surrounded by quite heavy traffic roads on the east, south and south-west, with peaks of traffic between 06:00–07:00 UT and 20:00–22:00 UT. The site is in the plume of Paris during east-north-easterly winds, while the air is relatively clean during south-westerly to north-westerly winds. More details of the site can be found in Laville et al. (2009, 2011), and Loubet et al. (2011).

The experiment was carried out from 20 August to 30 August 2009, following cattle slurry application of 98.5 kg N-NH$_4$ ha^{-1} and incorporation by tillage at 5 cm depth on 5 August 2009. Wheat was harvested just before 31 July 2009. The surface was, therefore, a mix of bare soil and sparse wheat residues.

Meteorological variables were measured half-hourly: incident solar radiations (CM7B, Kipp & Zonen, NL), wind speed (cup anemometer, Cimel, FR) and direction (W200P, Campbell Sci. Inc., USA), air temperature and relative humidity (HMP-45, Vaisala, FI) and precipitations (ARG100, Campbell Sci. Inc., USA). Soil water content (TDR CS 616, Campbell Sci. Inc., USA) profiles were also measured at 5, 10, 20, 30, 50 and 90 cm depth. TDR probes were calibrated against soil core samples. The photolysis rate for NO$_2$ (j_{NO_2}) was measured with a filter radiometer (Meteorologie consult GmbH, Germany). In addition, slow response analysers measured O$_3$, NO and NO$_2$ mixing ratios at 1.6 m (Table 1).

Three methods were used to measure fluxes between the surface and the atmosphere, i.e., aerodynamic gradient (AGM), eddy-covariance (EC) and automatic chamber (CH) methods. The instrument fetches ranged from 100 m to more than 400 m. The footprint analysis using the model described by Neftel et al. (2008) (an "easy-to-use" version of the Korman and Meixner (2001) model) reported in Loubet

Table 1. Instruments used for O$_3$-NO-NO$_2$ measurements. The instrument characteristics are those given by the manufacturers.

Measurement method	Gas measured	Analyser	Instrument characteristics	Measurement height	Measurement principle	Measurement frequency
Aerodynamic Gradient Method	O$_3$	FOS, Sextant Technology Ltd, New Zealand	Noise (1σ): NA Detection limit ($\pm 2\sigma$): NA	0.2, 0.7 and 1.6 m sequentially	Chemiluminescence	5 Hz (fast sensor)
	NO	CLD780TR, Ecophysics, Switzerland	Noise (1σ): <0.5 % of signal or 0.025 ppb Detection limit ($\pm 2\sigma$): <0.02 ppb	0.2, 0.7 and 1.6 m sequentially	Chemiluminescence	5 Hz (fast sensor)
	NO$_2$	LMA 3D-NO$_2$, Unisearch Associates Inc., Ontario, Canada	Noise (1σ): 1.5 % of signal Detection limit ($\pm 2\sigma$): 0.05 ppb	0.2, 0.7 and 1.6 m sequentially	Chemiluminescence	5 Hz (fast sensor)
Eddy-Covariance Method	O$_3$	ATDD, NOAA, USA	Noise (1σ): NA Detection limit ($\pm 2\sigma$): NA	3.17 m	Chemiluminescence	20 Hz (fast sensor)
	O$_3$	O$_3$ 41M, Environnement SA, France	Noise (1σ): 0.5 ppb Detection limit ($\pm 2\sigma$): 1 ppb	3.17 m	UV absorption	0.1 Hz (slow sensor)
Automatic Chambers Method	NO	42 CTL, Thermo-Environmental Instruments Inc., USA	Noise (1σ): 0.5 ppb Detection limit ($\pm 2\sigma$): 1 ppb	Inside the chambers	Chemiluminescence	0.1 Hz (slow sensor)
	O$_3$	O$_3$ 41M, Environnement SA, France	Noise (1σ): 0.5 ppb Detection limit ($\pm 2\sigma$): 1 ppb	Inside the chambers	UV absorption	0.1 Hz (slow sensor)
Other	NO/NO$_2$	42i, Thermo-Environmental Instruments Inc., USA	Noise (1σ): 0.4 ppb Detection limit ($\pm 2\sigma$): 0.8 ppb	1.6 m	Chemiluminescence	0.1 Hz (slow sensor)
	O$_3$	O$_3$ 41M, Environnement SA, France	Noise (1σ): 0.5 ppb Detection limit ($\pm 2\sigma$): 1 ppb	1.6 m	UV absorption	0.1 Hz (slow sensor)

et al. (2011) at 3.17 m height indicated that up to 93 % (average on a 10 days running median) of the field was in the EC mast footprint in spring-summer. Thus, at least 93 % of the field was in the AGM mast footprint since it was lower (see Sect. 2.2) than the EC mast. Each measurement system as well as the flux calculations are explained in the following.

2.2 Aerodynamic gradient measurements

The aerodynamic gradient method was used to determine O$_3$-NO-NO$_2$ fluxes. The O$_3$-NO-NO$_2$ mixing ratio profile measurements consisted of three Teflon PFA (perfluoroalkoxy copolymer) sample lines, each 7 m long with internal diameter of 9.24 mm. The inlets were installed at 0.2, 0.7 and 1.6 metres above the ground. The geometric mean measurement height was 0.61 m. To avoid the condensation of water vapour and avoid photochemical reactions, the sample lines were slightly heated with copper-constantan thermocouples under 12 V voltage and protected from radiation, respectively. A flow rate of 40 l min^{-1} in each line was provided by a pump (SV 1010 B, Busch, Switzerland), establishing a turbulent flow regime in each line (Reynolds number = 5900). A subsample line (Teflon PFA, 3.96 mm internal diameter) was connected on each 7 m sample line and connected to a Teflon solenoid valve (NResearch, USA) allowing to sequentially select a sample line. The switch between each line was performed every 30 s. A purge time of 10 s was used to purge the subsample line and the analysers. The flow inside the subsample line was 7 l min^{-1}. The total lag time of the system was estimated theoretically as 1.6 s.

Mixing ratios were measured with fast chemiluminescent gas analysers for O$_3$ (FOS, Sextant Technology Ltd, New Zealand), NO (CLD780TR, Ecophysics, Switzerland) and NO$_2$ (LMA 3D-NO$_2$, Unisearch Associates Inc, Ontario, Canada) (Table 1). The fast chemiluminescent gas analysers for NO and NO$_2$ were already used and described in previous studies (e.g., Nikitas et al., 1997; Jones et al., 2000; Rummel et al., 2002; Bröske et al., 2003; Hall et al., 2008). For O$_3$, the fast chemiluminescent gas analyser is based on the chemiluminescence of a coumarin dye absorbed on silica gel reacting with ozone. The chemiluminescence is monitored with a very sensitive photomultiplier. A pump inside the instrument allows a constant flow rate of 2 l min^{-1} to be maintained. These instruments were placed in a thermostated box (34.0 ± 0.5 °C) (Fig. 1). For NO$_2$, an O$_3$ scrubber (Drummond Technology, Canada) was used to suppress the interference of O$_3$. The NO and NO$_2$ fast sensors were calibrated every 6 h with a GPT (Gas Phase Titration) unit (146C, Thermo-Environment, USA). For O$_3$, the fast O$_3$ sensor was calibrated every 6 h by regression between measurements of slow and fast O$_3$ sensor at 1.6 m. The flux calculation was performed for time intervals of 30 min. The flux (F_C) of the gas (C) was calculated with the AGM (see e.g., Sutton et al., 1993) from friction velocity (u_*) and the mixing ratio scaling parameter (C_*) as:

$$F_C = -u_* C_* \tag{1}$$

where u_* was measured by eddy-covariance (see Sect. 2.3) and C_* is defined from the stability corrected gradient of scalar mixing ratio (C) with height (z) as:

$$C_* = k \frac{\partial C}{\partial \left(\ln \left(z - d \right) - \Psi_{\mathrm{H}} \right)} \tag{2}$$
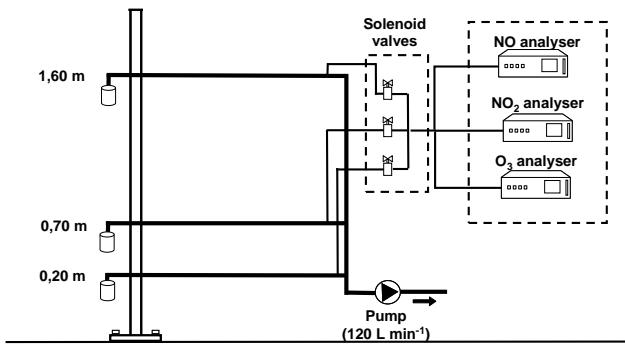
Fig. 1. Measurement set-up for the determination NO-O$_3$-NO$_2$ fluxes using aerodynamic gradient method.

where k is the von Kármán's constant (0.41), d the displacement height (m) assumed equal to zero for a bare soil and Ψ_H the integrated stability correction function for scalars (Dyer and Hicks, 1970).

The scaling parameter was determined based on the slope between C and $\ln(z-d)-\Psi_H$ using linear regression.

2.3 Eddy-covariance fluxes

Eddy-covariance is a direct measurement method to determine fluxes without application of any empirical constant (Foken, 2008). It has been extensively used to estimate turbulent fluxes of momentum, heat and trace gases (Aubinet et al., 2000; Running et al., 1999; Baldocchi et al., 2001; Dolman et al., 2006; Skiba et al., 2009) and is, thus, not detailed here. Briefly, the EC mast included a 3-D sonic anemometer (R3, Gill Inc., UK) and an open-path infrared absorption spectrometer for water vapour and CO$_2$ (IRGA 7500, LiCor, USA) located at 3.17 m height. Data were sampled and recorded at 50 Hz and the flux calculation was performed for 30 min intervals. Flux calculation and quality control were performed with the Edire software (Robert Clement, University of Edinburgh, UK) following the CarboEurope-IP methodology, which included a WPL (Webb-Pearman-Leuning) correction for the latent heat flux (Aubinet et al., 2000). From these measurements, the friction velocity (u_* in m s^{-1}) and the Obukhov length (L_O in m) were estimated as:

$$u_* = \left(-\overline{u'w'}\right)^{0.5} \tag{3}$$

$$L_O = \frac{u_*^3}{k \cdot g \left(\frac{-\overline{w'T_v'}}{T_v}\right)} \tag{4}$$

where w and u are the vertical and the longitudinal components of the wind velocity, respectively, g is the acceleration due to gravity (m s^{-2}), and T_v is the sonic temperature (K). The overbars and the primes denote the time average and the

fluctuation term, respectively. The O$_3$ flux was measured by EC using the Ratio Method described in Muller et al. (2010) by operating fast and slow response sensors at 3.17 m height simultaneously (Table 1).

2.4 Profile measurement analysis, AGM flux uncertainties and detection limits

The application of micrometeorological methods such as the AGM requires that the mixing ratios are stationary at each level. A stationarity test was, therefore, carried out on NO, O$_3$ and NO$_2$ mixing ratios to verify this prerequisite. The principle of this test is to divide the signal obtained over 30 min in j segments of i data samples and compare the standard deviation of the signal over each segment to the standard deviation over the 30 min period. For each sampling height, the segments correspond to the 20 s sampling period occurring every 1 min 30 s. For each segment, the standard deviation of the mixing ratio x is calculated as:

$$\sigma_j = \sqrt{\frac{\sum \left(x_i^2\right)}{n_i} - (\overline{x_i})^2} \tag{5}$$

The average standard deviation of the segments over 30 min is:

$$\sigma_{\text{segment}} = \frac{\sum \sigma_j}{n_j} \tag{6}$$

While over the entire 30 min period, the standard deviation is simply:

$$\sigma_{30\,\text{min}} = \sqrt{\frac{\sum_j \sum_i \left(x_{i,j}^2\right)}{j \cdot n_i} - (\overline{x_{30\,\text{min}}})^2} \tag{7}$$

The stationarity index S_x is then calculated for each compound x as:

$$S_x = 100 \cdot \left| \frac{\sigma_{30\,\text{min}} - \sigma_{\text{segment}}}{\sigma_{30\,\text{min}}} \right| \tag{8}$$

According to Foken and Wichura (1996), the data corresponding to $S_x \leq 30\%$ are of high quality, those with $30\% < S_x \leq 60\%$ have an acceptable quality, while those with $S_x > 60\%$ should be rejected.

The computation of the fluxes with AGM also requires a significant gradient of mixing ratios across heights. One useful indicator is the "gradient signal to noise ratio", which was estimated as the ratio of the average (ΔC) to the standard deviation (σ_C) of the mixing ratio difference between two successive levels (i.e., $\Delta C/\sigma_C$). The vertical mixing ratio gradient is significant if $\Delta C/\sigma_C > 1$ and conversely. This parameter evaluates the ability to resolve the vertical mixing ratio gradient based on real data, which integrates the analyser precision and the gradient representativeness over the background mixing ratio fluctuation.

Another way to determine whether vertical mixing ratio gradients are significant is to perform a statistical test. For each 30 min period, a two-sample unpaired Student's t-test (with a 95 % confidence interval) was performed to evaluate whether the average mixing ratios measured at (i) 0.2 and 0.7 m, (ii) 0.7 and 1.6 m, or (iii) 0.2 and 1.6 m, had significantly different averages. If both height (i) and height (ii) passed the t-test the flux was calculated using the three levels. If either height (i) or height (ii) failed the t-test, but height (iii) passed the t-test, the flux was calculated using levels 0.2 and 1.6 m only. Otherwise, the flux was considered non-significantly different from zero. It must be noted that unpaired Student's t-test can be only used for independent data, which in our case requires that we sample the data at a frequency smaller than the inverse of the integral time scale τ_I (Lenschow et al., 1994). The integral time scale τ_I was calculated using Edire software.

The relative uncertainty of the AGM flux for non-reactive cases was expressed as:

$$\frac{\sigma_{F_C}}{F_C} = \sqrt{\left(\frac{\sigma_{u*}}{u_*}\right)^2 + \left(\frac{\sigma_{C*}}{C_*}\right)^2} \qquad (9)$$

where σ represents standard deviations. The standard deviation of u_* was estimated based on the approach of Richardson et al. (2006) derived from the basic equations of turbulence:

$$\frac{\sigma_{u*}}{u_*} = \left[\left(\frac{2 \cdot \tau_t}{t}\right)^{0.5} \cdot \left(\frac{1 + \left(\overline{w'u'}\big/\sigma_w\sigma_u\right)^2}{\left(\overline{w'u'}\big/\sigma_w\sigma_u\right)^2}\right)^{0.5}\right]^{0.5} \qquad (10)$$

where τ_t is the integral timescale (i.e., the integral of the auto-correlation function) of the vertical wind velocity, t is the averaging time (1800 s) and σ_w and σ_u are the standard deviations of w and u, respectively.

The standard deviation of C_* (σ_{C*}) was determined as the standard deviation of the slope between C and $(\ln(z-d) - \Psi_H)$ by linear regression. However, in order to include the uncertainty in both C and Ψ_H, the linear regression was performed every 30 min on a randomly chosen dataset $[N(C, \sigma_C), \Psi_H(N(u_*, \sigma_{u*}))]$ with a number of data chosen to represent the number of independent data acquired with the fast sensors (at a frequency smaller than the inverse of the integral time scale τ_I).

The flux detection limit was determined empirically as the sum of the intercept of the linear regression between σ_{F_C} and F_C and the standard deviation of the intercept.

2.5 Flux divergence due to chemical reactions

Nitric oxide, NO$_2$ and O$_3$ are subject to (photo-) chemical reactions, thus, leading to chemical sources and sinks of these gases within the layer represented by the measurements. These chemical sources and sinks lead in turn to a vertical flux divergence between the surface and the measurement height, which should be taken into account if one is looking for the ecosystem flux. This is true, for instance, when studying O$_3$ impacts on plants, since the real O$_3$ flux experienced by the plant may not be that measured at a certain height above the surface. This is also valid for NO when comparing NO fluxes measured with chambers and those measured with EC or the AGM. According to Remde et al. (1993) and Warneck (2000), the main gas phase reactions for the NO-O$_3$-NO$_2$ triad are:

$$NO + O_3 \rightarrow NO_2 + O_2 \ k_r \qquad (R1)$$

$$NO_2 + O_2 + h\nu \rightarrow NO + O_3 \ j_{NO_2} \qquad (R2)$$
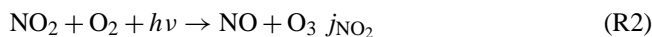
where k_r (=44.4 $\exp(-1370/(T_a + 273.15))$) in ppm^{-1} s^{-1}, e.g., Walton et al., 1997) and j_{NO_2} are the rate coefficient and the photolysis frequency for Reactions (1) and (2), respectively.

A simple method based on mass conservation for NO-O$_3$-NO$_2$ triad, proposed by Duyzer et al. (1995), was used to calculate the NO, O$_3$ and NO$_2$ flux divergences. This method calculates the flux F_{corr} at z_0 (corrected for chemical interactions) using the flux $F_{z=z_{ref}}$ estimated at z_{ref} (assuming that there was no chemical interaction at all). According to the simple equations for the flux derived by Lenschow and Delany (1987), Duyzer et al. (1995) demonstrated that, for heights lower than 4 m, the general form of the flux divergence is:

$$\left(\partial F / \partial z\right)_z = a\ln(z) + b \qquad (11)$$

The factors a for NO$_2$, NO and O$_3$ are calculated as:

$$a_{NO_2} = -a_{NO} = -a_{O_3} = -\frac{\phi_X}{ku_*}$$
$$\left[k_r\left([\overline{NO}] \cdot F_{O_3, z=z_{ref}} + [\overline{O_3}] \cdot F_{NO, z=z_{ref}}\right)\right.$$
$$\left. - j_{NO_2} \cdot F_{NO_2, z=z_{ref}}\right] \qquad (12)$$

where $[\overline{NO}]$ and $[\overline{O_3}]$ are mixing ratios at the geometric mean height of the profile measurements and $\phi_X = \phi_{NO} = \phi_{O_3} = \phi_{NO_2} = \phi_H$ is the stability correction function for heat (Dyer and Hicks, 1970; Webb, 1970). As shown by Lenschow and Delany (1987), the flux divergence at higher levels approaches zero. The factor b was calculated for NO$_2$, NO and O$_3$ as $b = -a\ln(z_2)$, where $z_2 = 1.6$ m, hence assuming that at $z = 1.6$ m the flux divergence was zero. This assumption was made since measurements at higher heights were not available. For each compound, the flux at z_0 (F_{corr}) is then approximated as:

$$F_{corr} = F_{z_1} + \int_{z_1}^{z_0} \left(\frac{\partial F}{\partial z}\right)_z dz$$
$$= F_{z=z_{ref}} + az_1\left(1 + \ln\left(z_2/z_1\right)\right) \qquad (13)$$

2.6 Turbulent transport and chemical reaction times

The comparison between the turbulent and the chemical time scales indicates if chemical reactions may occur during the transport of chemical species and, therefore, whether these can be treated as passive scalar or not. The turbulent transport time (τ_{trans} in s) between the measurement height (z_m) and the ground surface was simply expressed as the transfer resistance through each layer multiplied by the layer height (Garland, 1977):

$$\tau_{trans} = R_a(z) \times (z_m - z_0) + R_b \times (z_0 - z_{0'})$$
$$\approx R_a(z) \times (z_m - z_0) \tag{14}$$

$$R_a(z) = \frac{u(z)}{u_*^2} - \frac{\Psi_H(z/L) - \Psi_M(z/L)}{ku_*} \tag{15}$$

$$R_b = (B_{St} u_*)^{-1} \tag{16}$$

where $R_a(z)$ and R_b (s m^{-1}) are the aerodynamic resistance and quasi-laminar boundary layer resistance, respectively, calculated following Garland (1977), B_{St} is the Stanton number (dependent of the gas considered), u is the wind speed (m s^{-1}), Ψ_M the integrated stability correction function for momentum (Dyer and Hicks, 1970), and z_0 and $z_{0'}$ represent the roughness height for momentum and scalars (m), respectively. The contribution of the quasi-laminar boundary layer ($R_b \times (z_0 - z_{0'})$) was small (1.3 % $\pm$ 0.7 %) and was, therefore, neglected. The chemical reaction time for NO-O$_3$-NO$_2$ triad (τ_{chem} in s) gives the characteristic time scale of the set of reactions NO + O$_3$ → NO$_2$ + O$_2$ and NO$_2$ + O$_2$ + $h\nu$ → NO + O$_3$. This timescale is the time at which the O$_3$ concentration significantly changes from its "initial" value when reacting with NO and NO$_2$ (which also have an initial value and evolves). It can also be seen as the time required for reaching a new photo-stationary state following a change in the concentrations of NO, NO$_2$ or O$_3$ or the reaction constants k or J_{NO_2}. It was evaluated at the measurement height following the approach of Lenschow (1982) as:

$$\tau_{chem} = 2 / \left[j_{NO_2}{}^2 + k_r^2 \left([\overline{O_3}] - [\overline{NO}] \right)^2 \right.$$
$$\left. + 2 j_{NO_2} k_r \left([\overline{O_3}] + [\overline{NO}] + 2[\overline{NO_2}] \right) \right]^{0.5} \tag{17}$$

Based on this expression, the chemical depletion times for NO, O$_3$ and NO$_2$ were estimated as the asymptotic limits of Eq. (17) when either NO, O$_3$ or NO$_2$ mixing ratio was becoming the dominant specie (see also De Arellano and Duynkerke, 1992):

$$\tau_{deplNO} = \frac{1}{k_r[\overline{O_3}]} \tag{18}$$

$$\tau_{deplO_3} = \frac{1}{k_r[\overline{NO}]} \tag{19}$$

$$\tau_{deplNO_2} = \frac{1}{j_{NO_2}} \tag{20}$$

The ratio between τ_{trans} and τ_{chem} is defined as the Damköhler number (DA) (Damköhler, 1940):

$$DA = \frac{\tau_{trans}}{\tau_{chem}} \tag{21}$$

2.7 Automatic chamber flux measurements

The automatic chamber method was used to determine NO emissions from soil. Details can be found in Laville et al. (2011). Briefly, 6 automatic chambers in stainless steel (0.7 m × 0.7 m in area and 0.2 m height) measured continuously NO fluxes. The chambers were closed in sequence for 15 min each. The complete duration of one measurement cycle was, therefore, 1h 30 min. The NO and O$_3$ mixing ratios inside the chambers were measured using slow sensors (Table 1). The fluxes of NO without corrections for chemical reactions were calculated as:

$$F_{NO} = \frac{V}{A} \frac{\partial[NO]}{\partial t} \tag{22}$$

where F_{NO} is the NO flux, V the chamber headspace volume, A the ground area covered by the chamber and $\partial[NO]/\partial t$ the time derivative of the NO mixing ratio. The NO flux was determined during the first 3 min after chamber closure. Because of the long residence time of the air in the head space of the chamber, the NO fluxes need to be corrected for reactions with O$_3$ and NO$_2$. This was done following Laville et al. (2011), based on measurements of NO, NO$_2$ and O$_3$. As the chambers were opaque to solar radiation, only the reaction between NO and O$_3$ was considered and the photolysis of NO$_2$ was ignored. The corrected NO flux from chamber method is given as:

$$F_{NO_{corr}} = \frac{V}{A} \left(\frac{\partial[NO]}{\partial t} + k_r \cdot [NO] \cdot [O_3] \right) \tag{23}$$

3 Results

3.1 Overview on meteorological conditions, mixing ratios and AGM fluxes of O$_3$, NO and NO$_2$

The experimental period was quite sunny with global radiation reaching 800 W m^{-2} at noon, apart from 24 and 27 August, during which global radiation only reached 400 W m^{-2}. It rained on 24 August with a cumulated precipitation of 2 mm (Fig. 2a). The period was dry and warm. The relative humidity was around 80 % during night-time and decreased to about 30 % during daytime (Fig. 2b). Air temperature varied between 15 °C during night-time and 25 °C during daytime (Fig. 2c). During the measurement period, the
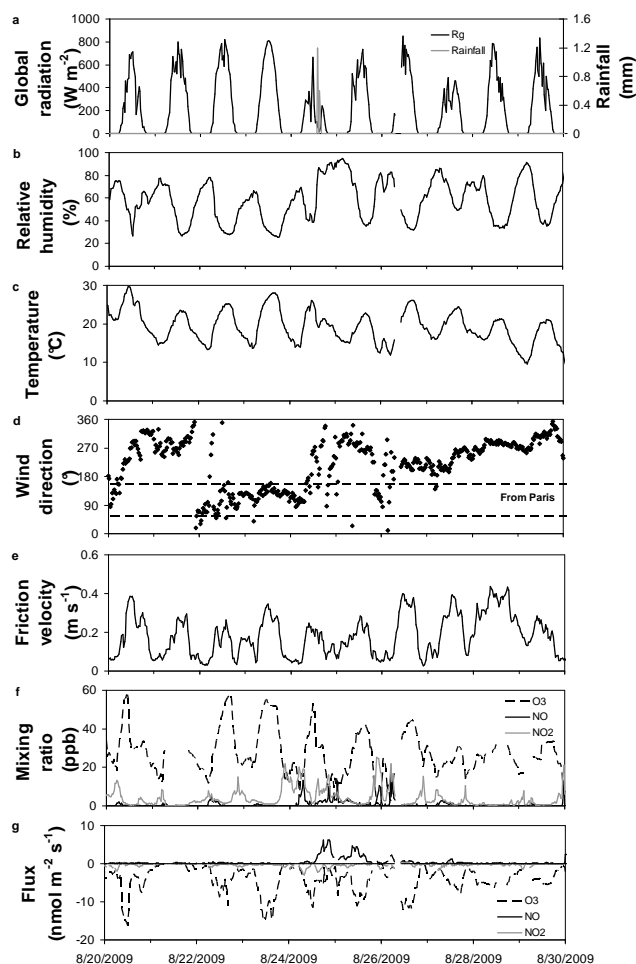
Fig. 2. Time series of **(a)** global radiation (black line) and rainfall (grey line), **(b)** air relative humidity, **(c)** air temperature, **(d)** wind direction, **(e)** friction velocity, **(f)** O_3 (dotted line), NO (black line) and NO_2 (grey line) mixing ratios and **(g)** O_3 (dotted line), NO (black line) and NO_2 (grey line) fluxes without chemical corrections determined by the AGM at $z = 0.61$ m. The fluxes were calculated without chemical corrections and tests on quality assurance. The dotted lines in panel **(d)** indicate winds coming from Paris.

wind blew from Paris from 22 and 24 August and during the nights of the 25 and 26 August (Fig. 2d). The WFPS (water-filled pore space) in the 0–10 cm top soil layer was around 29 % during the whole period.

During the measurement campaign, the friction velocity ranged from around $0.03 \, \text{m s}^{-1}$ during night-time to around $0.45 \, \text{m s}^{-1}$. The friction velocity showed a marked diurnal variation. It was at a minimum during night-time, increased during the morning to reach its maximum at noon and then decreased to its minimum during the afternoon. The second half of the measurement campaign (from 26 to 30 August 2009) was characterised by higher friction velocities than during the first part of the campaign, both during night-time and daytime (Fig. 2e).

The mixing ratios of O_3, NO and NO_2 featured a strong diurnal and day-to-day variation. The O_3 mixing ratios expectedly increased during the early morning to reach a maximum in the early afternoon. Night-time O_3 levels were between 0 and 30 ppb, whereas daytime levels were between 40 and 60 ppb. The O_3 mixing ratio variation between daytime and night-time was larger during the beginning, than towards the end of the experiment. The NO and NO_2 mixing ratio variations were markedly different: the minimum occurred during daytime and the maximum occurred during the early morning (between 05:00 and 07:30 UT) and the early evening (between 20:00 and 22:00 UT) during traffic peaks. The highest NO_x mixing ratios were observed during easterly winds, i.e., when air masses originated from the city of Paris. These mixing ratio peaks were less marked for NO than for NO_2, with NO_2 mixing ratio always greater than those of NO (Fig. 2f).

The fluxes of O_3, NO and NO_2 estimated using the aerodynamic gradient method are represented in Fig. 2g. These fluxes were uncorrected for chemical reactions, i.e., directly obtained using Eq. (1), and without any filtering based on stationarity tests or statistical tests. For O_3 and NO_2, deposition was observed, whereas NO was emitted from the ground. The O_3 flux showed a marked diurnal cycle. It increased during the early morning to reach a maximum at noon and then decreased to nearly zero during night. The NO flux was small during most of the measurement campaign, and peaked on 24 August and 25 following the rain event. The NO_2 flux had a less clear dynamics with alternating increases and decreases in the flux (Fig. 2g).

3.2 Mixing ratio gradients, quality analysis and AGM flux uncertainties

Nitric oxide (NO) mixing ratios measured with Thermo-Environmental 42i and CLD780TR agreed very well with a very small deviation of less than 1 % over the whole period, although the scatter was quite large at higher mixing ratios (Fig. 3). On the contrary, NO_2 mixing ratios measured with the Thermo-Environmental 42i were systematically higher, up to 25 % in mean over the whole period, than those measured with the LMA 3D-NO_2 (Fig. 3). We can hypothesise here that the large mixing ratios of NO (and NO_2) corresponded to advective situations. Under such situations, the plume emitted from the local traffic lines is not well mixed and, therefore, exhibits a large spatial and temporal variability in NO and NO_2 mixing ratios. Since the CLD780TR was sampling sequentially at the three levels, the mixing ratio measured at one level would miss some periods. Similarly, the 42i has an internal cycling and samples successively NO, NO_2 and a pre-chamber and, therefore, does not sample NO (NO_2 as well) all the time. Finally, the two analyser masts were located a few metres from each other and may have seen different NO concentrations in a non-well mixed plume.
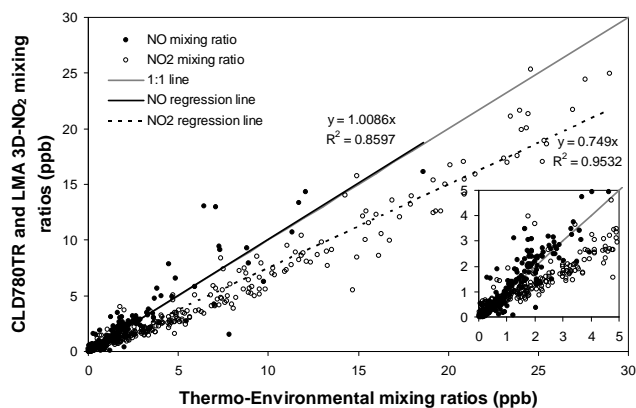
Fig. 3. Comparison of NO (black symbol) and NO$_2$ (open symbol) mixing ratios measured at 1.6 m height with Thermo-Environmental 42i and LMA 3D-NO$_2$ and CLD780TR. Grey line is the 1:1 line, black line the regression function for NO and dotted line the regression function for NO$_2$.

Table 2. Averaged mixing ratio difference measured between 1.6 m and 0.7 m and between 0.7 m and 0.2 m over the entire measurement period for O$_3$, NO and NO$_2$ and for different u_* classes.

	Mixing ratio difference between 1.6 m and 0.7 m (ppb)			Mixing ratio difference between 0.7 m and 0.2 m (ppb)		
u_*	O$_3$	NO	NO$_2$	O$_3$	NO	NO$_2$
0.05	2.11	−0.59	0.90	3.11	−0.71	1.68
0.15	0.97	−0.32	0.14	1.69	−1.27	0.37
0.25	0.77	−0.03	0.07	1.19	−0.06	0.13
0.35	0.98	−0.05	0.11	1.19	−0.02	0.09
0.45	0.32	−0.01	0.02	0.23	−0.05	0.04

For the three compounds, the mixing ratio difference between each level was dependent on u_* and increased when u_* decreased. Ozone mixing ratio gradients were quite large compared to NO and NO$_2$ mixing ratio gradients. Indeed, O$_3$ mixing ratio difference ranged from 0.32 ppb to 2.11 ppb between 0.7 m and 1.6 m and from 0.23 ppb to 3.11 ppb between 0.2 m and 0.7 m, while it only ranged from 0.01 to 1.68 ppb for NO and NO$_2$ whatever the levels. However, O$_3$ and NO$_2$ mixing ratios increased with height indicating deposition fluxes on average, whereas NO mixing ratio decreased with height indicating an emission flux on average (Table 2).

The "gradient signal to noise ratio" ($\Delta C/\sigma_C$) was found to be a good indicator of the quality of the mixing ratio gradients between the three levels. Indeed, for most of the data, $\Delta C/\sigma_C$ was larger than 1 when both the t-test indicated that mixing ratio where significantly different between both 0.2 m and 0.7 m, and 0.7 m and 1.6 m (95 % confidence interval). On the contrary, $\Delta C/\sigma_C$ was smaller than 1 when the t-test indicated that mixing ratios were not significantly different
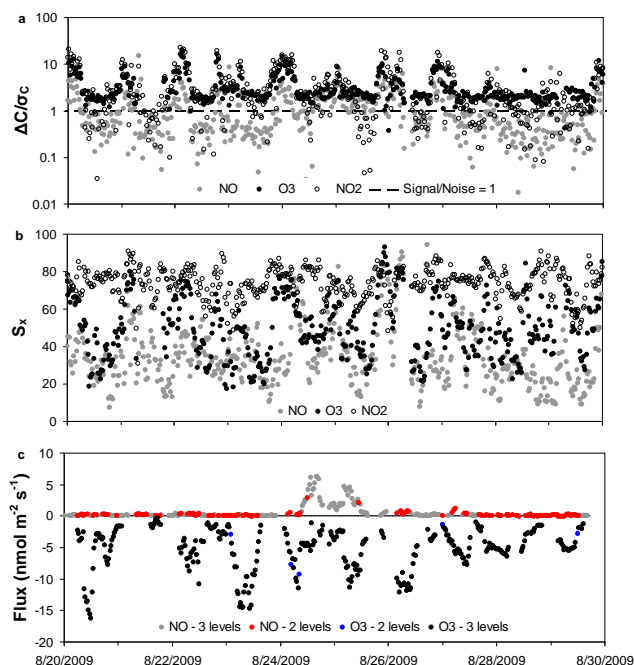

Fig. 4. Time series of (a) the "gradient signal to noise ratio" ($\Delta C/\sigma_C$) and (b) the stationarity index (S_x) for NO (grey symbols) O$_3$ (black symbols) and NO$_2$ (open symbols). The dotted line in panel (b) corresponds to a signal to $\Delta C/\sigma_C = 1$. (c) Time series of the fluxes determined by the AGM (without chemical corrections), satisfying both the stationarity test and the Student t-test. The flux was calculated either from 3 heights (grey symbols for NO; black symbols for O$_3$) or 2 heights (red symbols for NO; blue symbols for O$_3$) based on the t-tests (see text for details). Note that NO$_2$ fluxes are not represented because they failed both the t-test and stationarity test.

between at least two of the three levels (data not shown). The "gradient signal to noise ratio" showed a diurnal dynamics for the three gases: this ratio was higher during night-time and decreased during daytime, following the increase in turbulent mixing. For O$_3$, this ratio was systematically greater than 1, whereas for NO and NO$_2$ it was generally below 1 during daytime (except from 24 and 26 August for NO) and larger than 1 at night (Fig. 4a). It resulted in 93.5 % of the three-heights mixing ratio gradient was significantly different from zero for O$_3$, but only 50.2 % and 48.5 % for NO and NO$_2$. However, 98.5 %, 83.0 % and 82.7 % of the two-heights mixing ratio gradient (0.2 m and 1.6 m) were significantly different from zero for O$_3$, NO and NO$_2$, respectively (Table 3).

For NO$_2$, the mixing ratios were mostly non-stationary ($S_x > 60$ %) over the whole period. Only 6.1 % of the data satisfied the stationarity test (Fig. 4b and Table 3). For O$_3$ and NO, the stationarity test showed a diurnal cycle: S_x was higher during daytime and lower during night-time (Fig. 4b). It resulted that 72.2 % and 92.2 % of the data satisfied the stationarity test for O$_3$ and NO respectively (Table 3).

Table 3. Number of data available with significant mixing ratio gradients between the three measurement levels (i.e., 0.2 m 0.7 m and 1.6 m), with significant mixing ratio gradients only between the highest and lowest measurement height (i.e., 0.2 m and 1.6 m), and satisfying the stationarity test for O$_3$, NO and NO$_2$. The number of data satisfying both stationarity test and having significant mixing ratio gradients are also given. The percentage of data kept are indicated in brackets. The significance of mixing ratio gradients was established using Student's t-tests at the 95 % confidence interval.

|	O$_3$	NO	NO$_2$
No. of data available	443	476	476
Significant mixing ratio gradient between the 3 heights	414 (93.5 %)	239 (50.2 %)	231 (48.5 %)
Significant mixing ratios gradient only between 0.2 m and 1.6 m heights	22 (5.0 %)	156 (32.8 %)	163 (34.2 %)
Nb of data satisfying stationarity test ($S_x < 60$ %)	320 (72.2 %)	439 (92.2 %)	29 (6.1 %)
Stationarity test and significant gradient between the three heights	311 (70.2 %)	230 (48.3 %)	17 (3.6 %)
Stationarity test and significant gradient between 0.2 m and 1.6 m heights	5 (1.1 %)	146 (30.7 %)	9 (1.9 %)
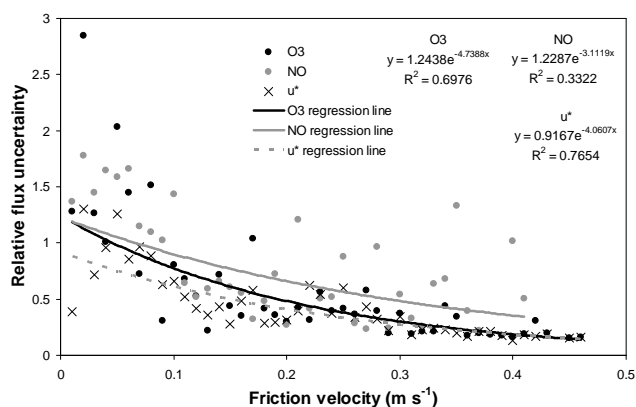
Fig. 5. Relative flux uncertainty as a function of friction velocity for O$_3$ (black circles), NO (grey circles), and u_* (crosses). Black line, grey line and dotted line are regressions for O$_3$, NO and u_*, respectively. The size of the bins used for averaging is 0.01 m s^{-1}. Only data satisfying both stationarity test and having mixing ratio gradients between the three levels above the detection limit were used. Since NO$_2$ failed both tests it is not represented here.

The percentage of AGM fluxes passing the stationarity test and for which the three-level mixing ratio gradient was significantly different from zero was 70.2 % for O$_3$, 48.3 % for NO and 3.6 % for NO$_2$. If the two-level mixing ratio gradient (0.2 and 1.6 m) is considered, the percentage of good quality data was 71.3 % for O$_3$, 79.0 % for NO and 5.5 % for NO$_2$ (Table 3 and Fig. 4c). Since not enough NO$_2$ fluxes satisfying quality tests were obtained, the NO$_2$ fluxes were not discussed in the following.

The relative uncertainty of the AGM fluxes decreased exponentially with increasing friction velocity (Fig. 5). The relative flux uncertainties ranged from 100–200 % for the lowest u_* to around 20 % (O$_3$) and 40 % (NO) for the highest u_*. The relative u_* uncertainty ranged from 90 % to 15 % whereas the relative C_* uncertainty varied from 110 % to 5 % (O$_3$) and 35 % (NO).

Based on the standard deviation of the flux, the flux detection limit was estimated as 0.08 nmol m^{-2} s^{-1} for O$_3$ and 0.22 nmol m^{-2} s^{-1} for NO.

3.3 Flux divergences due to chemical reactions

The fluxes at z_0 with chemical corrections, i.e., corrected from chemical reactions in the air column, were calculated as described in Sect. 2.5. However, the method used required NO, O$_3$ and NO$_2$ fluxes. As indicated previously, NO$_2$ fluxes did not pass the quality tests and the NO$_2$ flux divergence was, therefore, not analysed. Nevertheless, we hypothesized that the magnitude of the NO$_2$ fluxes was, however, correct in order to establish and discuss the flux divergence for O$_3$ and NO.

The fluxes at z_0 with chemical corrections calculated using Eq. (13) were higher than those without chemical correction at $z = 0.61$ m for NO, whereas they were lower for O$_3$. The absolute chemical correction was 0.12 nmol m^{-2} s^{-1} on average for both NO and O$_3$, but could reach 1.44 nmol m^{-2} s^{-1} during the NO emission peak (24 and 25 August). Due to differences in fluxes magnitude, the weight of the chemical correction term on the flux was different for NO and O$_3$: chemical corrections accounted for less than 1 % for O$_3$, while it was around 10 % for NO, when averaged over the experimental campaign. For NO, the flux difference increased markedly and could reach up to 80 % when the Damköhler number became greater than unity (see Fig. 6). Such conditions typically occurred between 19:00 and 04:30 UT.

The comparison between the chemical reaction time of the NO-O$_3$-NO$_2$ triad and the chemical depletion times for NO, O$_3$ and NO$_2$ showed that τ_{chem} was particularly close to τ_{deplNO}, whereas τ_{deplO3} and τ_{deplNO2} were always much larger than τ_{chem} (Fig. 7).
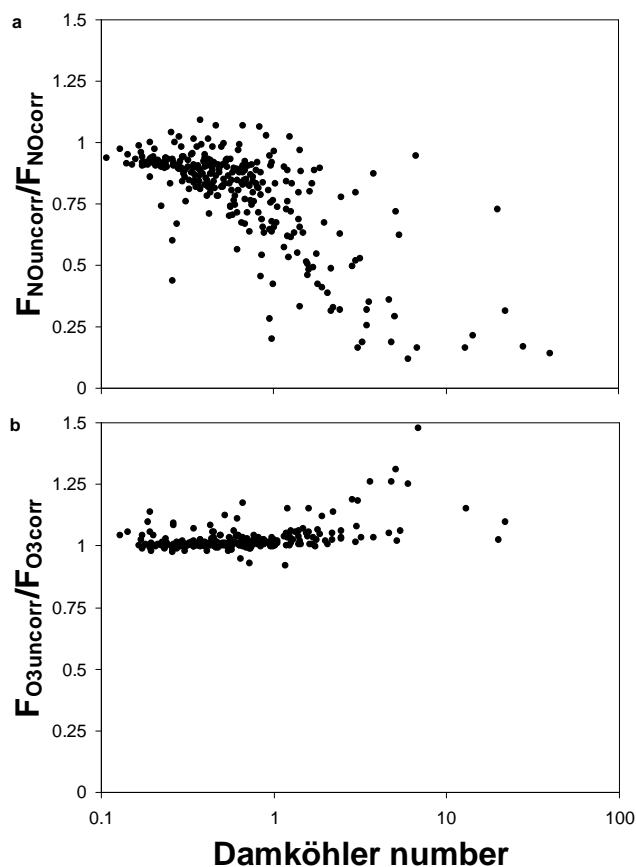
Fig. 6. Ratio of fluxes without to fluxes with chemical corrections as a function of the Damköhler number for **(a)** NO and **(b)** O₃.

4   Discussion

4.1   Quality of NO-O₃-NO₂ AGM fluxes

One critical point when using the aerodynamic gradient method is to measure the mixing ratios of gases at different heights with sufficient accuracy and precision. Nitric oxide mixing ratios measured with the CLD780TR analyser agreed very well with the Thermo-Environmental 42i, whereas NO₂ mixing ratios from the Thermo-Environmental 42i were larger than with the LMA 3D-NO₂ (Fig. 3). The Thermo-Environmental 42i uses a molybdenum converter heated at 325 °C to convert NO₂ to NO and evaluate NO₂ mixing ratio by the difference between NO$_x$ and NO mixing ratios. This catalytic conversion is unfortunately not specific to NO₂. Several compounds as peroxyacetyl nitrate (PAN), nitrous acid (HONO), HNO₃ and organic nitrates are also converted to NO and, therefore, induce an overestimation of the NO₂ mixing ratio (Parrish and Fehsenfeld, 2000; Dari-Salisburgo et al., 2009). The interference using a molybdenum converter could be as large as 50 % of the apparently measured NO₂ mixing ratio in some reported studies (Dunlea et al., 2007). The LMA 3D-NO₂ measures the chemi-
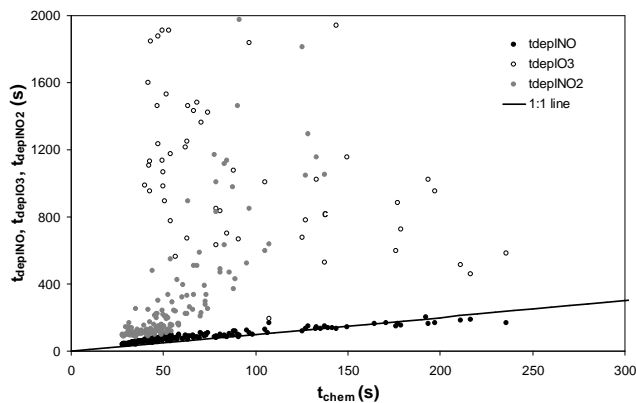

Fig. 7. Comparison between chemical reaction time for the set of chemical reactions of the NO-O₃-NO₂ triad (τ_{chem}) and chemical depletion times for NO (black symbols), O₃ (open symbols) and NO₂ (grey symbols). The black line corresponds to the 1:1 line.

luminescence produced by the reaction between NO₂ and an alkaline luminal solution. The only interference reported is with O₃, quoted as less than 1 %, and PAN, quoted at 25 % of the equivalent mixing ratio of NO₂ (Nikitas et al., 1997). However, the LMA 3D-NO₂ was used with an O₃ scrubber, and the fact that the analyser with the molybdenum sensor gave larger mixing ratios rather suggests that the Thermo-Environmental 42i was subject to positive interferences, probably due to the presence of other reactive nitrogen species (NO$_y$), although the LMA 3D-NO₂ could be subject to PAN interference as indicated previously.

The application of the AGM requires that (i) the mixing ratio gradient is above the detection limit, and that (ii) the mixing ratios are stationary. The gradient detection limit was evaluated with the "gradient signal to noise ratio" ($\Delta C/\sigma_C$), as well as with an unpaired t-test evaluating if the averaged mixing ratio at two levels were significantly different. For O₃ the three-height mixing ratio gradient was most of the time above the detection limit as shown by $\Delta C/\sigma_C > 1$ and by the t-test approach. On the contrary, for NO and NO₂, the three-heights mixing ratio gradient was above the detection limit only during 50 % of the time, as shown by the t-test as well as by $\Delta C/\sigma_C$, which was above 1 only during night-time (Fig. 4, Table 3). For NO and NO₂, the two-heights mixing ratio gradient was, however, above the detection limit during 80 % of the time (Table 3).

Although the gradient system was shown to be adapted for measuring mixing ratio gradients above the detection limit, (for three or at least two levels), the stationarity criteria was not met for all gases. For NO and O₃, the mixing ratios were generally stationary during daytime and non-stationary during night-time (Fig. 4b), which results from the intermittency of the turbulence during night-time. For NO₂, the mixing ratios were systematically non-stationary ($S_x > 60$) with even larger S_x values at night. During night-time the NO₂ non-stationarity was also caused by the turbulence

intermittency, as suggested by the similar S_x found for O$_3$, NO and NO$_2$ at night (Fig. 4b). However, during daytime, the non-stationarity of NO$_2$ cannot be explained by the turbulent regime, as the same turbulence is experienced by O$_3$ and NO, which are stationary. It can be reasonably hypothesized that the non-stationarity of NO$_2$ mixing ratios during daytime was due to local advection: the NO emitted by traffic road located at a few hundreds of metres rapidly reacted with O$_3$ to form NO$_2$ and was advected, leading to non-stationarity in NO$_2$ mixing ratios.

The combination of stationarity tests and gradient detection limit criteria led to a rejection of 94.5 % of the NO$_2$ fluxes and only 28.7 % and 21 % of O$_3$ and NO fluxes measured by the AGM. However, for this latter it must be noted that up to 50 % of the data would be rejected if we had calculated fluxes based on three levels instead two levels (0.2 and 1.6 m). This larger noise in the NO and NO$_2$ gradients was both due to a combination of small fluxes (Fig. 2) and large local advection from the nearby traffic lines. Indeed, since (i) the O$_3$ flux is larger than NO and NO$_2$ fluxes and (ii) the lifetime of O$_3$ is greater than those of NO and NO$_2$ (Logan, 1983), the O$_3$ mixing ratios are expected to show larger gradient and smaller fluctuations than NO and NO$_2$. Thus, in this study the quality of AGM was perturbed by local advection (dominant for NO$_2$) and (ii) the magnitude of the fluxes (dominant for NO).

The relative uncertainty of O$_3$ and NO fluxes was dependent on the friction velocity and ranged from 150–200 % at low u_* to 20 % (O$_3$) and 40 % (NO) at high u_* (Fig. 5). The relative uncertainties on the flux were a combination of the uncertainty on u_* and on the mixing ratio gradient. Indeed, the uncertainty on the mixing ratio gradient contributed to σ_{C*}/C_* while u_* contributed (i) on the one hand to σ_{u*}/u_* and (ii) on the other hand to σ_{C*}/C_* (i.e., in the Ψ_H function through Obukhov length estimation). Thus, when u_* was low, typically during night-time, the uncertainty on the mixing ratio gradient was small and of similar magnitude for O$_3$ and NO, but the uncertainty on u_* was large and dominated the uncertainty on the flux (Fig. 4a). On the contrary, when u_* was large, the uncertainty on both u_* and the mixing ratio gradients contributed equally to the flux uncertainties. This also explains why the O$_3$ flux uncertainty was nearly two times lower than the NO flux uncertainty at large u_*: when u_* was large, the O$_3$ flux was much larger than the NO flux which led to a larger mixing ratio gradient and a lower uncertainty (as illustrated by the differences in $\Delta C/\sigma_C$) (Table 2).

The large number of mixing ratio points available to evaluate the mixing ratio at each level using fast sensors is beneficial in diminishing the flux uncertainty. Figure 8a shows indeed that the relative flux uncertainty diminishes with the number of measurement points per level over a 30 min period. In the present study, the use of fast response sensor provided approximately 2000 measurements per level per 30 min. However, Fig. 8a is constructed assuming that all points are independent (any cross-correlation between the
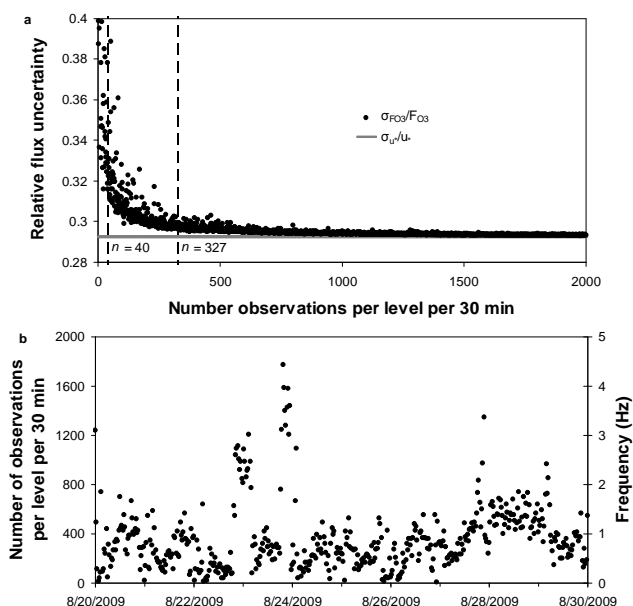

Fig. 8. (a) Relative flux uncertainty for the aerodynamic gradient method as a function of the number of mixing ratio data available per level per 30 min. Example of the O$_3$ flux the 25 August 2009 from 15:30 to 16:00. The number of points available from measurements using the fast response sensor ($n = 327$) and under the hypothesis of the use of slow response sensor ($n = 40$) are indicated on the figure with the dashed line. **(b)** Time series of number of mixing ratio points used to estimate the mean mixing ratio at each level per 30 min based on the frequency corresponding to the inverse of the integral time scale of turbulence. This frequency corresponds to the maximum frequency above which the data are not independent and should not contribute to diminish the standard deviation as shown in **(a)**.

data is equal to zero). Since by definition, the integral time scale τ_I is the time over which the turbulent signal is correlated to itself (Lenschow et al., 1994), the number of independent points to be considered are those points sampled at a frequency $f_I = \tau_I^{-1}$. In the example considered in Fig. 8a, the number of point was evaluated as 327 per level per 30 min. The resulting relative flux uncertainty is quite close to the minimal one, i.e., around 30 % for the example considered. Under the hypothesis of the use of slow response sensor, only 40 measurements per level per 30 min would be available, which corresponded to a relative flux uncertainty ranging from 35 % up to 40 %. In addition, the term σ_{u*}/u_* is constant and was equal to 30 % in the example considered, and the term σ_{C*}/C_* is equal to 10 % to 20 % for 40 measurements per level per 30 min and equal to 5 % for 327 measurements per level per 30 min. Thus, the use of fast sensor allowed to diminish the relative C_* uncertainty by decreasing the σ_{C*} value, by a factor 2 to 4 for the example considered here. However, over the whole campaign, the use of fast response sensors was only beneficial during daytime when the friction velocity was high and the integral time scale was

Table 4. Relative difference between AGM fluxes (of O$_3$, NO and NO$_2$) determined using the stability functions proposed by Dyer and Hicks (1970) and those proposed by Businger et al. (1971) and modified by Högstrom (1988). Positive values indicate greater fluxes using the stability functions proposed by Dyer and Hicks (1970).

	O$_3$	NO	NO$_2$
1st Quartile	+6.4 %	+5.9 %	+6.3 %
Median	+9.4 %	+9.3 %	+9.5 %
3rd Quartile	+14.5 %	+14.4 %	+14.8 %

small (Fig. 8b). From the overall look at the dataset, we find that an acquisition frequency of around 1.2 Hz would have been optimum in our case (Fig. 8b). This conclusion would change depending on the average u_* at the site studied.

In spite of the possibility to decrease the relative flux uncertainties by increasing the acquisition frequency, it must be kept in mind that one important source of uncertainty is the choice of the stability functions to calculate fluxes from the AGM. In this study, the stability functions proposed by Dyer and Hicks (1970) were used, but several others exist, in particular the stability functions proposed by Businger et al. (1971) and modified by Högstrom (1988). Table 4 shows that the O$_3$, NO and NO$_2$ fluxes estimated using stability functions proposed by Dyer and Hicks (1970) were systematically greater (by roughly 10 % on average) than those obtained using the stability functions proposed by Businger et al. (1971) and modified by Högstrom (1988). For 25 % of the time, the Dyer and Hicks formulation can even be up to 14 % to 15 % larger than the Businger/Högstrom formulation.

4.2 Influence of chemical reactions

The fluxes of reactive species in the surface boundary layer may diverge with height due to chemical reactions. For the NO-O$_3$-NO$_2$ triad, this was shown in previous studies (Kramm et al., 1996; Walton et al., 1997). However, if only the NO$_x$-O$_3$ triad is considered, the mass conservation lead to height invariant-fluxes of NO$_x$ (NO + NO$_2$) and O$_x$ (NO$_2$ + O$_3$) (Kramm et al., 1996; Walton et al., 1997).

The flux divergence due to chemical interactions was estimated as 0.12 nmol m^{-2} s^{-1} on average for NO and O$_3$. However, this flux divergence was typically negligible for O$_3$ as it accounted for around 1 % of the O$_3$ flux on average, whereas for NO it was 10 % of the flux. Indeed, the O$_3$ flux (mean: -4.27 nmol m^{-2} s^{-1}) was roughly ten times higher than the NO flux (mean: 0.41 nmol m^{-2} s^{-1}). The same result was reported by Galmarini et al. (1997) during an experimental study, for which there was no substantial difference between O$_3$ and inert species fluxes, whereas NO flux divergence was strongly affected by chemistry.

At the half-hourly time scale, the flux divergence was highly variable and could reach 25 % for O$_3$ and up to 80 % for NO (Fig. 6). The flux divergence for the two gases was dependent on the Damköhler number. The chemical reaction time was similar to the chemical depletion time for NO, whereas the chemical depletion times for NO$_2$ and O$_3$ were systematically higher (Fig. 7). This result demonstrates that the flux divergence was mainly due to the reaction between NO and O$_3$ and was limited by NO which mixing ratio was the lowest, but was not caused by NO$_2$ photolysis. During the campaign, O$_3$ mixing ratios ranged between 15 ppb ($\sim 6.2 \times 10^2$ nmol m^{-3}) and 60 ppb ($\sim 24.9 \times 10^2$ nmol m^{-3}), whereas NO mixing ratios only ranged between 1 ppb ($\sim 0.4 \times 10^2$ nmol m^{-3}) and 10 ppb ($\sim 4.2 \times 10^2$ nmol m^{-3}) (Fig. 2f). In addition, the reaction between NO and O$_3$ is a second order reaction, but in this study it could be approximated by a pseudo-first order reaction since O$_3$ was most of the time in excess when compared to NO. The pseudo-first order reaction rate constant could be defined as $k'_r = k_r \cdot \overline{[O_3]}$ (in s^{-1}).

The flux divergence sharply increased, especially for NO, when the Damköhler number became greater than 1, i.e., when the turbulent transport time was larger than the chemical reaction time (Fig. 6). This typically occurred during night-time, when the friction velocity was very low, and the turbulent transport time very large. Under such conditions NO reacted with O$_3$ inducing large chemical flux divergences. The largest flux divergence (1.44 nmol m^{-2} s^{-1}) was observed during the night between 24 and 25 August 2009, i.e., when the soil NO emission was large and O$_3$ flux was relatively small. For DA < 0.1, i.e., when turbulent transport is much faster than the chemical transformation time, there is not enough time for the chemical reactions to occur during the transport and the chemical flux divergence is small. However, for 0.1 < DA < 1, chemical reactions are still expected to induce a flux divergence. In that range the flux divergence ranged between 0 % and 25 % of the surface flux (Fig. 6a). Near the ground, O$_3$ mixing ratios were lower and NO mixing ratios higher than those at the mean geometrical height. Thus, NO emitted from soil could rapidly react with O$_3$ to form NO$_2$, which induced a divergence in O$_3$ and NO fluxes near the ground.

4.3 Comparison of AGM fluxes with EC O$_3$ and automatic chambers NO fluxes

There are only few studies reporting comparisons of measurement methods, especially for O$_3$ and NO$_x$, and most of them do not account for the chemical flux divergence.

Ozone fluxes measured using the aerodynamic gradient method showed a reasonable agreement with O$_3$ fluxes measured by eddy-covariance (Fig. 9). Over the whole period, the difference between EC and AGM O$_3$ fluxes was only about 1 % which is in the range of the O$_3$ flux uncertainty. However, at the half-hourly scale the difference between EC and AGM fluxes was around 31 %, but could reach up to 200 %, especially when fluxes were particularly small. Indeed, for the
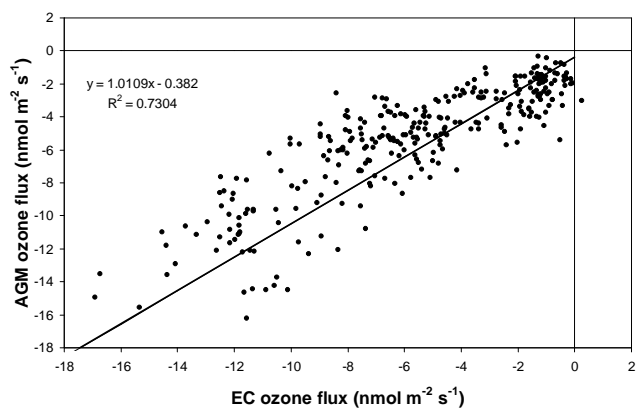
Fig. 9. Comparison between O_3 fluxes measured using aerodynamic gradient method and eddy-covariance method. The measured fluxes were corrected for chemical reactions.
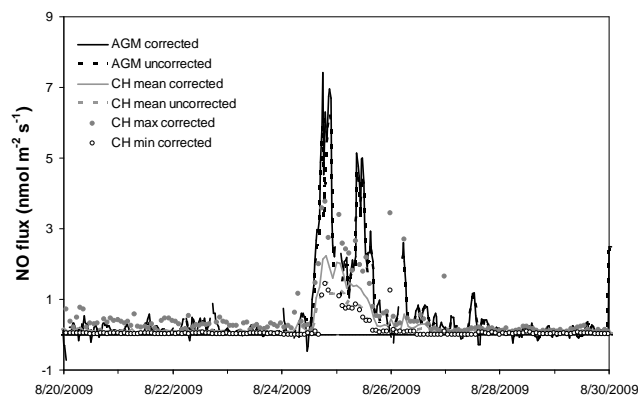

Fig. 10. Comparison between NO fluxes measured by the aerodynamic gradient method (black line) and automatic chambers (grey line). Solid and dotted lines are fluxes with and without corrections for chemical reactions, respectively. Grey and open symbols are respectively maximal and minimal NO fluxes measured by automatic chambers.

lowest fluxes, i.e., smaller than $-2\,\mathrm{nmol\,m^{-2}\,s^{-1}}$, O_3 fluxes from eddy-covariance measurements were smaller compared to AGM fluxes. These conditions typically corresponded to night-time when small u_* occurred. It is well recognised that eddy-covariance method underestimates fluxes during nocturnal conditions with low u_* (Goulden et al., 1996; Gu et al., 2005; Moureaux et al., 2006). Many reasons, such as drainage and intermittent turbulent transfer in time and space (Massman and Lee, 2002), could explain the underestimation of O_3 fluxes using the EC method, leading to the discrepancy with the AGM flux measurements. It is also very well known that AGM fluxes are subject to large uncertainties under stable conditions (Foken, 2008).

The comparison between NO fluxes measured using automatic chambers and AGM method showed a good correlation. However, NO fluxes measured by chambers were nearly five times smaller than those measured by AGM during the large NO emission peak between 24 and 26 August 2009 without corrections for chemical reactions (Fig. 10). It resulted that the difference between NO fluxes estimated from AGM and chambers was around $0.45\,\mathrm{nmol\,m^{-2}\,s^{-1}}$ on average, but could reach $6\,\mathrm{nmol\,m^{-2}\,s^{-1}}$. Chemical reactions explained only a part of this discrepancy. For the chamber method, the chemical correction term accounted for $0.13\,\mathrm{nmol\,m^{-2}\,s^{-1}}$ on average over the whole period, but could reach $0.92\,\mathrm{nmol\,m^{-2}\,s^{-1}}$ during the NO emission peak. These values are comparable to the chemical flux divergence estimated with the AGM (i.e., $0.12\,\mathrm{nmol\,m^{-2}\,s^{-1}}$ on average and $1.44\,\mathrm{nmol\,m^{-2}\,s^{-1}}$ at maximum). Even with chemical corrections, the chamber NO fluxes were still three times lower than the AGM fluxes during the large NO emission between 24 and 26 August 2009, with a maximal absolute difference between the two methods that reached $5.3\,\mathrm{nmol\,m^{-2}\,s^{-1}}$ (Fig. 10). However, it must be noted that the chemical correction we used for chambers measurements only takes into account the chemical reaction between NO and O_3. Indeed, other compounds could react with NO

in the chamber headspace, such as peroxy radicals, which could lead to underestimates of NO fluxes using the chamber method. In addition to chemical reactions in the chamber, other reasons could explain the difference between NO fluxes measured by chambers and AGM methods. On the one hand, it is well known that NO emissions are quite heterogeneous as shown by the large difference between maximal and minimal NO fluxes measured by the 6 automatic chambers (Fig. 10). It seems, however, that spatial variability could not explain solely the difference as the maximal NO fluxes measured by chambers were still twice as small as the AGM NO fluxes during the peak NO emission. However, it must be noted that chamber measurements were not in the AGM footprint, even if the nitrogen treatment was the same for the whole field. Thus, it was possible that in the AGM footprint, NO emissions were greater than in the area where the automatic chambers were installed. On the other hand, the increase in NO emissions followed a weak rainfall event on 24 August 2009, with only 2 mm cumulated. The NO emission was, thus, enhanced by a small increase in humidity at the soil surface. Since this rainfall event was short, it was likely that chambers did not receive the same amount of water because of the chamber cover. Thus, the soil surface inside the chambers may be not in the same hydric state as outside, limiting soil NO emission and leading to underestimation of NO fluxes using chamber method. Finally, it must be kept in mind that the discrepancy between AGM and chamber method for NO flux measurements could be linked with limitations of the AGM: for heterogeneous fluxes such as NO fluxes, the different heights (i.e., 0.2 m, 0.7 m and 1.6 m) had not the same footprint and, therefore, the mixing ratios at each height is influenced by different areas of the field which may have different soil NO emission. Indeed, the soil NO emissions measured by the chamber showed a large spatial

variability at the local scale (around 60 % for a few metres). However, heterogeneities at larger scales (a few tens to hundreds of metres) are also expected because of the soil, water and biomass heterogeneity (see Loubet et al., 2011). The other limitations of the AGM were discussed at length in previous sections and could also explain part of the discrepancy.

5   Summary and conclusions

The study reports measurements of NO, O$_3$ and NO$_2$ fluxes using the aerodynamic gradient method. The mixing ratio profile measurements were done using fast response sensors. The experiment was performed over an agricultural field during a period with bare soil, from 20 August to 30 August 2009. The aim of this study was to evaluate flux measurements using the AGM, to understand to which extent NO, O$_3$ and NO$_2$ fluxes were affected by chemical reactions and to compare them to results from dynamic chambers and the EC method.

A special attention was focussed on mixing ratio measurements, significance of mixing ratio gradients and quality of AGM fluxes. The comparison of mixing ratios measured with slow and fast response sensors showed a good agreement between the instruments, except for NO$_2$. The conversion of NO$_2$ to NO using a molybdenum converter heated at 325 °C is not specific to NO$_2$ explaining the observed overestimation of NO$_2$ by the Thermo-Environmental 42i. Owing to the high accuracy and fast response of the chemiluminescent NO, O$_3$ and NO$_2$ analysers, the gradient system was capable of detecting significant differences between mixing ratio measured at the three sampling heights, or at least between the highest and the lowest sampling height. In spite of the high accuracy of mixing ratio gradient measurements, the NO$_2$ mixing ratios were subject to large non-stationary due to local advection of road traffic emissions. This led to the rejection of the NO$_2$ fluxes calculated from the AGM. It was shown that the AGM flux uncertainty was caused by a combination of uncertainty in the friction velocity and the mixing ratio gradients. The relative flux uncertainties ranged from 150–200 % for the lowest u_* to around 20 % and 40 % for O$_3$ and NO, respectively, for the highest u_*. However, the use of a fast sensor allowed diminishing the uncertainty. The flux detection limits of the AGM were estimated as 0.08 nmol m^{-2} s^{-1} for O$_3$ and 0.22 nmol m^{-2} s^{-1} for NO.

Flux divergences due to chemical reactions were only 1 % for O$_3$, but around 10 % for NO. In addition, the flux divergence of NO increased when the chemical time scale became smaller than the turbulent transport time and could reach 80 %. It was evaluated that the flux divergence was due to the reaction between NO and O$_3$, where NO is the limiting compound. This study showed that above a bare soil, when O$_3$ fluxes are significantly higher than NO and NO$_2$ fluxes, the impact of chemistry upon O$_3$ fluxes could be neglected, in contrary to NO fluxes.

The aerodynamic gradient and eddy-covariance methods were found to give similar results for O$_3$ fluxes except during night-time conditions with low friction velocities affecting both EC and AGM fluxes measurements. The NO fluxes determined with the dynamic chamber method were lower than those obtained by the AGM, with a maximum difference between the two methods of about 6 nmol m^{-2} s^{-1} without chemical correction and 5.3 nmol m^{-2} s^{-1} including the correction for chemical reactions in the chamber headspace, due to heterogeneous soil NO emissions and a probable perturbation of the soil surface by the presence of chambers.

Thus, this study showed that, contrary to the comparison reported by Muller et al. (2010), the O$_3$ fluxes measured by AGM and EC are reliable, supporting the results obtained by Keronen et al. (2003). According to the results obtained, it is recommended to use specific gas analysers and to use fast response sensors to limit the uncertainty in flux measurements using profile methods. Although fast response sensors are usually used for EC measurements, their application to AGM measurements could represent a valuable alternative to estimate fluxes of chemically reactive species, which require flux and mixing ratio measurements at several heights. Finally, fast response chemiluminescent analysers are subject to less interference than slow response analysers (e.g., water vapor for O$_3$ UV absorbance analysers (Wilson and Birks, 2006); PAN, HONO, HNO$_3$ and organic nitrates for slow NO$_2$ analysers based on catalytic conversion with molybdenum converter (Dunlea et al., 2007)), allowing accurate mixing ratio measurements.

References

Ainsworth, E. A.: Rice production in a changing climate: a meta-analysis of responses to elevated carbon dioxide and elevated ozone concentration, Global Change. Biol., 14, 1642–1650, 2008.

Altimir, N., Tuovinen, J. P., Vesala, T., Kulmala, M., and Hari, P.: Measurements of ozone removal by Scots pine shoots: calibration of a stomatal uptake model including the non stomatal component, Atmos. Environ., 38, 2387–2398, 2004.

Altimir, N., Kolari, P., Tuovinen, J.-P., Vesala, T., Bäck, J., Suni, T., Kulmala, M., and Hari, P.: Foliage surface ozone deposition: a role for surface moisture?, Biogeosciences, 3, 209–228, doi:10.5194/bg-3-209-2006, 2006.

Aneja, V. P. and Robarge, W. P.: Soil-biogenic NO$_x$, emissions and air quality, in: Preservation of Our World in the Wake of Change, edited by: Steinberger, Y., Vol. VIA, Israel Society for Ecology, 50–52, 1996.

Aubinet, M., Grelle, A., Ibrom, A., Rannik, U., Moncrieff, J., Foken, T., Kowalski, A. S., Martin, P. H., Berbigier, P., Bernhofer, C., Clement, R., Elbers, J., Granier, A., Grunwald, T., Morgenstern, K., Pilegaard, K., Rebmann, C., Snijders, W., Valentini, R., and Vesala, T.: Estimates of the annual net carbon and water exchange of forests: The EUROFLUX methodology, Adv. Ecol. Res., 30, 113–175, 2000.

Baldocchi, D. D., Falge, E., Gu, L., Olson, R., Hollinger, D., Running, S., Anthoni, P., Bernhofer, C., Davis, K., Evans, R., Fuentes, J., Goldstein, A., Katul, G., Law, B., Lee, X., Malhi, Y., Meyers, T., Munger, W., Oechel, W., Paw U, K. T., Pilegaard, K., Schmid, H. P., Valentini, R., Verma, S., Vesala, T., Wilson, K., and Wofsy, S.: FLUXNET: A New Tool to Study the Temporal and Spatial Variability of Ecosystem-Scale Carbon Dioxide, Water Vapor and Energy Flux Densities, B. Am. Meteorol. Soc., 82, 2415–2434, 2001.

Bröske, R., Kleffmann, J., and Wiesen, P.: Heterogeneous conversion of NO$_2$ on secondary organic aerosol surfaces: A possible source of nitrous acid (HONO) in the atmosphere?, Atmos. Chem. Phys., 3, 469–474, doi:10.5194/acp-3-469-2003, 2003.

Businger, J. A., Wyngaard, J. C., Izumi, Y., and Bradley, E. F.: Flux-profile relationships in the atmospheric surface layer, J. Atmos. Sci., 28, 181–189, 1971.

Butterbach-Bahl, K., Breuer, L., Gasche, R., Willibald, G., and Papen, H.: Exchange of trace gases between soils and the atmosphere in Scots pine forest ecosystems of the northeastern German lowlands. 1. Fluxes of N$_2$O, NO/NO$_2$ and CH$_4$ at forest sites with different N-deposition, Forest. Ecol. Manag., 167, 123–134, 2002.

Coyle, M., Nemitz, E., Storeton-West, R., Fowler, D., and Cape, J. N.: Measurements of ozone deposition to a potato canopy, Agr. Forest. Meteorol., 149, 655–666, 2009.

Damköhler, G.: Der Einfluss der Turbulenz auf die Flammengeschwindigkeit in Gasgemischen, Z. Elektrochem. Angew. P., 46, 601–652, 1940.

Dari-Salisburgo, C., Di Carlo, P., Giammaria, F., Kajii, Y., and D'Altorio, A.: Laser induced fluorescence instrument for NO$_2$ measurements: Observations at a central Italy background site, Atmos. Environ., 43, 970–977, 2009.

De Arellano, J. V. G. and Duynkerke, P. G.: Influence of chemistry on the flux-gradient relationships for the NO-O$_3$-NO$_2$ system, Bound. Lay. Meteorol., 61, 375–387, 1992.

Delmas, R., Serça, D., and Jambert, C.: Global inventory of NO$_x$ sources, Nutr. Cycl. Agroecosys., 48, 51–60, 1997.

Denman, K. L., Brasseur, G., Chidthaisong, A., Ciais, P., Cox, P. M., Dickinson, R. E., Hauglustaine, D., Heinze, C., Holland, E., Jacob, D., Lohmann, U., Ramachandran, S., da Silva Dias, P. S., Wofsy, S. C., and Zhang, X.: Couplings between changes in the climate system and biogeochemistry, in: Climate Change 2007: The Physical Science Basis, edited by: Solomon, S., Qin, D., Manning, M., Chen, Z., Marquis, M., Averyt, K. B., Tignor, M.,

and Miller, H. L., Contribution of Working Group I to the Fourth Assessment Report of the Intergovernmental Panel on Climate Change, Cambridge University Press, Cambridge, UK, and New York, NY, USA, 2007.

Denmead, O. T.: Approaches to measuring fluxes of methane and nitrous oxide between landscape and the atmosphere, Plant. Soil., 309, 5–24, 2008.

Dolman, A. J., Noilhan, J., Durand, P., Sarrat, C., Brut, A., Piguet, B., Butet, A., Jarosz, N., Brunet, Y., Loustau, D., Lamaud, E., Tolk, L., Ronda, R., Miglietta, F., Gioli, B., Magliulo, V., Esposito, M., Gerbig, C., Körner, S., Glademard, P., Ramonet, M., Ciais, P., Neininger, B., Hutjes, R. W. A., Elbers, J. A., Macatangay, R., Schrems, O., Pérez-Landa, G., Sanz, M. J., Scholz, Y., Facon, G., Ceschia, E., and Beziat, P.: The CarboEurope regional experiment strategy, B. Am. Meteorol. Soc., 87, 1367–1379, 2006.

Droppo, J.: Concurrent measurements of ozone dry deposition using eddy covariance and profile flux methods, J. Geophys. Res., 90, 2111–2118, 1985.

Dunlea, E. J., Herndon, S. C., Nelson, D. D., Volkamer, R. M., San Martini, F., Sheehy, P. M., Zahniser, M. S., Shorter, J. H., Wormhoudt, J. C., Lamb, B. K., Allwine, E. J., Gaffney, J. S., Marley, N. A., Grutter, M., Marquez, C., Blanco, S., Cardenas, B., Retama, A., Ramos Villegas, C. R., Kolb, C. E., Molina, L. T., and Molina, M. J.: Evaluation of nitrogen dioxide chemiluminescence monitors in a polluted urban environment, Atmos. Chem. Phys., 7, 2691–2704, doi:10.5194/acp-7-2691-2007, 2007.

Duyzer, J. H., Deinum, G., and Baak, J.: The interpretation of measurements of surface exchange of nitrogen oxides: correction for chemical reactions, Philos. T. Roy. Soc. A., 351, 231–248, 1995.

Dyer, A. J. and Hicks, B. B.: Flux-profile relationship in the constant flux layer, Q. J. Roy. Meteor. Soc., 96, 715–721, 1970.

Fang, S. and Mu, Y.: NO$_x$ fluxes from the three kinds of agricultural lands in the Yangtze Delta, China, Atmos. Environ., 41, 4766–4772, 2007.

Felzer, B. S., Cronin, T., Reilly, J. M., Melillo, J. M., and Wang, X.: Impacts of ozone on trees and crops, C. R. Geos., 339, 784–798, 2007.

Foken, T.: Micrometeorology, Springer, Verlag Berlin Heidelberg, 308 p., 2008.

Foken, T. and Wichura, B.: Tools for quality assessment of surface-based flux measurements, Agr. Forest. Meteorol., 78, 83–105, 1996.

Fowler, D., Flechard, C., Skiba, U., Coyle, M., and Cape, J. N.: The atmospheric budget of oxidized nitrogen and its role in ozone formation and deposition, New. Phytol., 139, 11–23, 1998.

Fowler, D., Cape, J. N., Coyle, M., Smith, R. I., Hjellbrekke, A. G., Simpson, D., Derwent, R. G., and Jonhson, C. E.: Modelling photochemical oxidant formation, transport, deposition and exposure of terrestrial ecosystems, Environ. Pollut., 100, 43–55, 1999.

Galmarini, S., De Arellano, J. V. G., and Duyzer, J.: Fluxes of chemically reactive species inferred from mean concentration measurements, Atmos. Environ., 31, 2371–2374, 1997.

Garland, J. A.: The dry deposition of sulphur dioxide to land and water surface, Proc. R. Soc. Lon. A. Mat., 354, 245–268, 1997.

Gerosa, G., Marzuoli, R., Cieslik, S., and Ballarin-Denti, A.: Stomatal ozone fluxes over barley field in Italy, "Effective exposure" as a possible link between exposure- and flux-based approaches, Atmos. Environ., 38, 2421–2432, 2004.

Goulden, M. L., Munger, J. W., Fan, S. M., Daube, B. C., and Wofsy, S. C.: Measurements of carbon sequestration b long-term eddy-covariance: methods and critical evaluation of accuracy, Glob. Change. Biol., 2, 169–182, 1996.

Gu, L., Falge, E. M., Boden, T., Baldocchi, D. D., Black, T. A., Saleska, S. R., Suni, T., Verma, S. B., Vesala, T., Wofsy, S. C., and Xu, L.: Objective threshold determination for night-time eddy flux filtering, Agr. Forest. Meteorol., 128, 179–197, 2005.

Hall, S. J., Huber, D., and Grimm, N. B.: Soil N$_2$O and NO emissions from an arid, urban ecosystem, J. Geophys. Res., 113, G01016, doi:10.1029/2007JG000523, 2008.

Högström, U.: Non-dimensional wind and temperature profiles in the atmospheric surface layer: A re-evaluation, Bound.-Lay. Meteorol., 42, 55–78, 1988.

IPCC: Climate Change, The Scientific Basis. Contribution of Working Group I to the Fourth Assessment Report of Intergovernmental Panel on Climate Change (IPCC), Cambridge University Press, Cambridge, UK and New York, NY USA, 2007.

Jones, A. E., Weller, R., Wolff, E. W., and Jacobi, H. W.: Speciation and rate of photochemical NO and NO$_2$ production in Antarctic snow, Geophys. Res. Lett., 27, 345–348, 2000.

Keronen, P., Reissel, A., Rannick, U., Pohja, T., Siivola, E., Hiltunen, V., Hari, P., Kulmala, M., and Vesala, T.: Ozone flux measurements over a Scots pine forest using eddy covariance method: performance evaluation and comparison with flux-profile method, Boreal. Environ. Res., 8, 425–443, 2003.

Korman, R. and Meixner, F. X.: An analytical footprint model for non-neutral stratification, Bound.-Lay. Meteorol., 99, 207–224, 2001.

Kramm, G., Müller, H., Fowler, D., Höfken, K., Meixner, F. X., and Schaller, E.: A Modified Profile Method for Determining the Vertical Fluxes of NO, NO$_2$, Ozone, and HNO$_3$ in the Atmospheric Surface Layer, J. Atmos. Chem., 13, 265–288, 1991.

Kramm, G., Dlugi, R., Dollard, G. J., Foken, T., Mölders, N., Müller, H., Seiler, W., and Sievering, H.: On the dry deposition of ozone and reactive nitrogen species, Atmos. Environ., 29, 3209–3231, 1995.

Kramm, G., Beier, N., Foken, T., Müller, H., Schröder, P., and Seiler, W.: A SVAT Scheme for NO, NO$_2$ and O$_3$ – Model Description and Test Results, Meteorol. Atmos. Phys., 61, 89–106, 1996.

Lamaud, E., Carrara, A., Brunet, Y., Lopez, A., and Druilhet, A.: Ozone fluxes above and within a pine forest canopy in dry and wet conditions, Atmos. Environ., 36, 77–88, 2002.

Lamaud, E., Loubet, B., Irvine, M., Stella, P., Personne, E., and Cellier, P.: Partitioning of ozone deposition over a developed maize crop between stomatal and non-stomatal uptakes, using eddy-covariance flux measurements and modelling, Agr. Forest. Meteorol., 149, 1385–1386, 2009.

Laville, P., Flura, D., Gabrielle, B., Loubet, B., Fanucci, O., Rolland, M. N., and Cellier, P.: Characterisation of soil emissions of nitric oxide at field and laboratory scale using high resolution method, Atmos. Environ., 43, 2648–2658, 2009.

Laville, P., Lehuger, S., Loubet, B., Chaumartin, F., and Cellier, P.: Effect of management, climate and soil conditions on N$_2$O and NO emissions from an arable crop rotation using high temporal resolution measurements, Agr. Forest. Meteorol., 151, 228–240, 2011.

Lenschow, D. H.: Reactive Trace Species in the Boundary Layer from a Micrometeorological Perpective, J. Meteorol. Soc. Jpn., 60, 472–480, 1982.

Lenschow, D. H. and Delany, A. C.: An analytic formulation for NO and NO$_2$ flux profiles in the atmospheric surface layer, J. Atmos. Chem., 5, 301–309, 1987.

Lenschow, D. H., Mann, J., and Kristensen, L.: How long is long enough when measuring fluxes and other turbulence statistics, J. Atmos. Ocean. Technol., 11, 661–673, 1994.

Li, D. and Wang, X.: Nitric oxide emission from a typical vegetable field in the Pearl River Delta, China, Atmos. Environ., 41, 9498–9505, 2007.

Logan, J. A.: Nitrogen oxides in the troposphere: Global and regional budgets, J. Geophys. Res., 88, 785–807, 1983.

Loubet, B., Laville, P., Lehuger, S., Larmanou, E., Flechard, C., Mascher, N., Genermont, S., Roche, R., Ferrara, R. M., Stella, P., Personne, P., Durant, B., Decuq, C., Flura, D., Masson, S., Fanucci, O., Rampon, J. N., Siemens, J., Kindler, R., Gabrielle, B., and Cellier, P.: Carbon, nitrogen and Greenhouse gases budgets over a four years crop rotation in northern France, Plant. Soil., 343, 109–137, 2011.

Massman, W. J. and Lee, X.: Eddy covariance flux corrections and uncertainties in long-term studies of carbon and energy exchanges, Agr. Forest. Meteorol., 113, 121–144, 2002.

Meixner, F. X., Fickinger, Th., Marafu, L., Serça, D., Nathaus, F. J., Makina, E., Mukurumbira, L., and Andreae, M.O.: Preliminary results on nitric oxide emission from a southern African savanna ecosystem, Nutr. Cycl. Agroecosys., 48, 123–138, 1997.

Mikkelsen, T. N., Ro-Poulsen, H., Pilegaard, K., Hovmand, M. F., Jensen, N. O., Christensen, C. S., and Hummelshoej, P.: Ozone uptake by an evergreen forest canopy: temporal variation and possible mechanisms, Environ. Pollut., 109, 423–429, 2000.

Milford, C., Theobald, M. R., Nemitz, E., Hargreaves, K. J., Horvath, L., Raso, J., Dämmgen, U., Neftel, A., Jones, S. K., Hensen, A., Loubet, B., Cellier, P., and Sutton, M. A.: Ammonia fluxes in relation to cutting and fertilization of an intensively managed grassland derived from an inter-comparison of gradient measurements, Biogeosciences, 6, 819–834, doi:10.5194/bg-6-819-2009, 2009.

Moureaux, C., Debacq, A., Bodson, B., Heinesch, B., and Aubinet, M.: Annual net ecosystem carbon exchange by a sugar beet crop, Agr. Forest. Meteorol., 139, 25–39, 2006.

Muller, J. B. A., Coyle, M., Fowler, D., Gallagher, M. W., Nemitz, E. G., and Percival, C. J.: Comparison of ozone fluxes over grassland by gradient and eddy covariance technique, Atmos. Sci. Lett., 10, 164–169, 2009.

Muller, J. B. A., Percival, C. J., Gallagher, M. W., Fowler, D., Coyle, M., and Nemitz, E.: Sources of uncertainty in eddy covariance ozone flux measurements made by dry chemiluminescence fast response analysers, Atmos. Meas. Tech., 3, 163–176, doi:10.5194/amt-3-163-2010, 2010.

Neftel, A., Spirig, C., and Ammann, C.: Application and test of a simple tool for operational footprint evaluations, Environ. Pollut., 152, 644–652, 2008.

Nikitas, C., Clemitshaw, K. C., Oram, D. E., and Penkett, S. A.: Measurements of PAN in the Polluted Boundary Layer and Free Troposphere Using a Luminol-NO$_2$ Detector Combined with a Thermal Converter, J. Atmos. Chem., 28, 339–359, 1997.

Paoletti, E.: Ozone slows stomatal response to light and leaf wounding in a Mediterranean evergreen broadleaf, Arbutus unedo, Environ. Pollut., 134, 439–445, 2005.

Paoletti, E. and Grulke, N. E.: Does living in elevated CO_2 ameliorate tree response to ozone? A review on stomatal response, Environ. Pollut., 137, 483–493, 2005.

Parrish, D. D. and Fensenfeld, F. C.: Methods for gas-phase measurements of ozone, ozone precursors and aerosol precursors, Atmos. Environ., 34, 1921–1957, 2000.

PORG: Ozone in the UK (4th report of the Photochemical Oxidants Review Group), Department of the Environment, Transport and the Regions, London (ITE Edinburgh), 1997.

Remde, A., Ludwig, J., Meixner, F. X., and Conrad, R.: A study to explain the emission of nitric oxide from a marsh soil, J. Atmos. Chem., 17, 249–275, 1993.

Richardson, A. D., Hollinger, D. Y., Burba, G. G., Davis, K. J., Flanagan, L. B., Katul, G. G., Munger, J. W., Ricciuto, D. M., Stoy, P. C., Suyker, A. E., Verma, S. B., and Wofsy, S. C.: A multi-site analysis of random error in tower-based measurements of carbon and energy fluxes, Agr. Forest. Meteorol., 136, 1–18, 2006.

Rummel, U., Ammann, C., Gut, A., Meixner, F. X., and Andreae, M. O.: Eddy covariance measurements of nitric oxide flux within an Amazonian rain forest, J. Geophys. Res.-Atmos., 107, 8050, doi:8010.1029/2001JD000520, 2002.

Rummel, U., Ammann, C., Kirkman, G. A., Moura, M. A. L., Foken, T., Andreae, M. O., and Meixner, F. X.: Seasonal variation of ozone deposition to a tropical rain forest in southwest Amazonia, Atmos. Chem. Phys., 7, 5415–5435, doi:10.5194/acp-7-5415-2007, 2007.

Running, S. W., Baldocchi, D. D., Turner, D. P., Gower, S. T., Bakwin, P. S., and Hibbard, K. A.: A global terrestrial monitoring network integrating tower fluxes, flask sampling, ecosystem modelling and EOS satellite data, Remote Sens. Environ., 70, 108–127, 1999.

Sanchez-Martin, L., Vallejo, A., Dick, J., and Skiba, U.: The influence of soluble carbon and fertilizer nitrogen on nitric oxide and nitrous oxide emissions from two contrasting agricultural soils, Soil. Biol. Biochem., 40, 142–151, 2008.

Sitch, S., Cox, P. M., Collins, W. J., and Huntingford, C.: Indirect radiative forcing of climate change through ozone effects on the land-carbon sink, Nature, 448, 791–795, 2007.

Skiba, U., Drewer, J., Tang, Y. S., van Dijk, N., Helfter, C., Nemitz, E., Famulari, D., Cape, J. N., Jones, S. K., Twigg, M., Pihlatie, M., Vesala, T., Larsen, K. S., Carter, M. S., Ambus, P., Ibrom, A., Beier, C., Hensen, A., Frumau, A., Erisman, J. W., Brüggemann, N., Gasche, R., Butterbach-Bahl, K., Neftel, A., Spirig, C., Horvath, L., Freibauer, A., Cellier, P., Laville, P., Loubet, B., Magliulo, E., Bertolini, T., Seufert, G., Andersson, M., Manca, G., Laurila, T., Aurela, M., Lohila, A., Zechmeister-Boltenstern, S., Kitzler, B., Schaufler, G., Siemens, J., Kindler, R., Flechard, C., and Sutton, M. A.: Biosphere-atmosphere exchange of reactive nitrogen and greenhouse gases at the NitroEurope core flux measurements sites: Measurement strategy and first data sets, Agr. Ecosyst. Environ., 133, 139–149, 2009.

Sutton, M. A., Fowler, D., and Moncrieff, J. B.: The exchange of atmospheric ammonia with vegetated surfaces. I: Unfertilized vegetation, Q. J. Roy. Meteor. Soc., 119, 1023–1045, 1993.

Vingarzan, R.: A review of surface ozone background levels and trends, Atmos. Environ., 38, 3431–3442, 2004.

Walton, S., Gallagher, M. W., and Duyzer, J. H.: Use of a detailed model to study the exchange of NO_x and O_3 above and below a deciduous canopy, Atmos. Environ., 31, 2915–2931, 1997.

Warneck, P.: Chemistry of the Natural Atmosphere, 2nd Edn., International Geophysics Series. Academic Press Inc., San Diego, USA, 2000.

Webb, E. K.: Profile relationships: the log-linear range, and extension to strong stability, Q. J. Roy. Meteor. Soc., 106, 85–100, 1970.

Wilson, K. L. and Birks, J. W.: Mechanism and elimination of a water vapor interference in the measurement of ozone UV absorbance, Environ. Sci. Technol., 40, 6361–6367, 2006.

Wittig, V. E., Ainsworth, E. A., Naidu, S. L., Karnosky, D. F., and Long, S. P.: Quantifying the impact of current and future tropospheric ozone on tree biomass, growth, physiology and biochemistry: a quantitative meta-analysis, Global Change. Biol., 15, 396–424, 2009.

Yienger, J. J. and Levy, H.: Empirical model of global soil-biogenic NO_x emissions, J. Geophys. Res.-Atmos., 200, 11447–11464, 1995.

Zhang, L., Brook, J. R., and Vet, R.: On ozone dry deposition with emphasis on non-stomatal uptake and wet canopies, Atmos. Environ., 36, 4787–4799, 2002.

Zhang, L., Vet, R., Brook, J. R., and Legge, A. H.: Factors affecting stomatal uptake of ozone by different canopies and a comparison between dose and exposure, Sci. Total. Environ., 370, 117–132, 2006.